Journal of Mechanical, Civil and Industrial Engineering
ISSN: 2709-0809
DOI: 10.32996/jmcie
Journal Homepage: www.al-kindipublisher.com/index.php/jmcie

JMCIE
AL-KINDI CENTER FOR RESEARCH AND DEVELOPMENT

| RESEARCH ARTICLE

Machine Learning-Based Prediction of Porosity Formation in Laser Powder Bed Fusion of Mechanical Components

Matthew J. Reynolds[1], Emily R. Carter[2], Daniel T. Mitchell[3], and Lauren M. Brooks[4]
[1234] Mechanical Engineering Graduate Program, Purdue University, 610 Purdue Mall, West Lafayette, IN 47907, USA
Corresponding Author: Matthew J. Reynolds, **E-mail:** mjreynolds@purdue.edu

| ABSTRACT

Porosity remains one of the most persistent quality barriers in laser powder bed fusion (LPBF), especially for mechanical components that must satisfy fatigue, leak-tightness, and structural reliability requirements. This paper presents a machine learning framework for predicting LPBF porosity formation using process parameters, powder descriptors, and physically meaningful features such as volumetric, linear, and areal energy density. The study uses a literature-constrained benchmark dataset to demonstrate the workflow when proprietary in-situ and X-ray computed tomography data are not yet available. The modeling strategy compares logistic regression, support vector machine, gradient boosting, random forest, and neural-network classifiers for high-porosity risk prediction, while a random-forest regressor estimates porosity percentage. The results indicate that tree-based ensemble learning provides the strongest balance between accuracy, recall, and interpretability, with volumetric energy density, scan speed, oxygen level, and powder morphology emerging as influential predictors. The discussion connects these model behaviors to lack-of-fusion, keyhole, spatter, and gas-entrapment mechanisms. Overall, the manuscript argues that reliable porosity prediction should not rely on machine settings alone. A more useful approach combines physics-guided feature engineering, sensor-informed data streams, cross-validated learning, and explainability tools to support inspection prioritization and eventual closed-loop process control.

| KEYWORDS

laser powder bed fusion; porosity prediction; machine learning; additive manufacturing; melt pool monitoring; process optimization; defect detection

| ARTICLE INFORMATION

ACCEPTED: 10 March 2026 **PUBLISHED:** 26 April 2026 **DOI:** 10.32996/jmcie.2026.7.3.4

1. Introduction

Laser powder bed fusion has become a leading metal additive manufacturing route for high-value mechanical components because it can create lightweight geometries, integrated features, internal passages, and customized material layouts that are difficult to produce using conventional subtractive or forming methods (Frazier, 2014; Herzog et al., 2016; DebRoy et al., 2018). In practical production, however, the value of geometric freedom is limited if the internal quality of the component cannot be controlled. Porosity is especially important because even a small volume fraction of defects can reduce fatigue life, introduce leak paths, and create uncertainty during qualification. The main pore families are usually described as lack-of-fusion pores caused by insufficient melting, gas-related pores associated with powder or shielding conditions, and keyhole pores produced when excessive energy destabilizes the melt pool.

The difficulty is that pore formation is controlled by interacting thermal, fluid-flow, metallurgical, and machine-control phenomena. Laser power, scan speed, hatch spacing, layer thickness, powder packing, local heat accumulation, oxygen level, and scan-path history can all affect the same melt track. High-speed imaging and X-ray studies have shown that vapor-cavity instability, melt-pool collapse, powder motion, and rapid solidification can occur within very short time scales, which explains

why a parameter set that appears acceptable in one build may behave differently in another (King et al., 2014; Cunningham et al., 2019; Zhao et al., 2020). A reliable prediction method therefore needs to recognize both the average process window and the local process context.

Machine learning offers a practical route to convert heterogeneous LPBF data into risk predictions, but it should not be used as a simple black-box replacement for metallurgical reasoning. The most useful models translate raw machine inputs into engineering features, learn nonlinear relationships from inspection-labeled data, and return explanations that can be understood by process engineers. Prior studies on layerwise imagery, melt-pool signatures, and physics-informed porosity prediction show that this combined approach is more credible than using process parameters alone (Scime & Beuth, 2018; Smoqi et al., 2022). The present paper builds on that direction by developing a transparent framework for predicting both high-porosity risk and porosity percentage.

The specific objective is to design and evaluate a prediction workflow that can be adapted to experimental LPBF datasets from in-situ sensing and post-build inspection. The study contributes a physically guided feature set, a reproducible calculation procedure, a comparative model assessment, and an interpretation strategy for engineering decision support. The framework is also positioned within the broader movement toward smart manufacturing, where real-time monitoring, predictive maintenance, digital twins, and process quality control are connected rather than handled as separate activities (Hossain et al., 2021, 2024; Hossain & Bhuiyan, 2025).

2. Literature Review

2.1 Porosity mechanisms in LPBF

LPBF porosity is usually interpreted through the competing effects of insufficient fusion, stable conduction melting, excessive keyhole melting, powder-bed disturbance, and gas entrapment. Lack-of-fusion pores form when the melt pool does not penetrate deeply enough or overlap sufficiently with neighboring tracks, leaving irregular voids that can be highly damaging under cyclic loading. Keyhole pores, by contrast, are associated with high energy input and vapor-driven depression of the melt surface; when the depression becomes unstable and collapses, a void can be trapped below the solidifying surface (Zhang et al., 2017; Martin et al., 2019). These mechanisms are different, but both can appear in the same build if the local thermal condition changes from region to region.

Melt-pool physics also includes denudation, spatter, recoil pressure, Marangoni flow, and rapid solidification. Denudation and vapor micro-jets can redistribute powder near the track, while spatter can remove material from the intended scan path and disturb subsequent layers (Matthews et al., 2016; Ly et al., 2017). These phenomena matter because machine learning features based only on nominal power and speed may not capture the real material state at the point of melting. When a model includes powder descriptors, scan-context variables, or sensor-derived signals, it has a better chance of recognizing the process conditions that create these transient defects.

Materials and component design further influence defect tolerance. Multi-material, functionally graded, lightweight, and fire-resistant alloy systems may bring advantages for mechanical and thermal applications, but they also introduce thermal-gradient mismatch, interfacial instability, and property variation that must be considered during process qualification (Hossain et al., 2023, 2024, 2026). Residual stress and distortion are also connected to porosity because local overheating, scan strategy, and heat accumulation can influence both pore formation and dimensional stability. A prediction framework for mechanical components should therefore support not only density improvement but also reliability, manufacturability, and downstream inspection planning.

2.2 In-situ monitoring and defect detection

In-situ monitoring has advanced from simple machine-log recording to high-speed imaging, thermography, photodiode sensing, optical emission spectroscopy, acoustic emission, and X-ray-assisted validation. Review studies emphasize that these methods are useful because they capture thermal and optical signatures before final inspection, but the signal alone is not enough; it must be aligned with scan position, layer number, build geometry, and ex-situ ground truth (Tapia & Elwany, 2014; Everton et al., 2016; Grasso & Colosimo, 2017). This alignment is often the most time-consuming part of building a reliable machine-learning dataset.

The strongest experimental evidence for pore formation comes from synchrotron X-ray imaging and high-speed diagnostics. These measurements reveal melt-pool shape, keyhole dynamics, powder motion, and vapor-driven instability in real time, providing a physical basis for feature engineering rather than leaving the model to infer everything from raw labels (Cunningham et al., 2019; Zhao et al., 2020). Thermography and pyrometry are more practical for industrial machines because they can be applied across many layers and many parts, although their signals normally require careful calibration and position-based registration.

Layerwise image analysis has become a particularly important branch of LPBF monitoring because it can be deployed within commercial machine workflows. Computer-vision models can identify recoater streaks, powder-bed irregularities, missing material, spatter accumulation, and unusual layer texture before destructive inspection is performed (Gobert et al., 2018; Snow et al., 2021). Deep-learning approaches can extend this capability, but they must be validated carefully so that the model does not simply memorize one machine, alloy, camera angle, or build layout.

2.3 Machine learning and physics-guided modeling

The most reliable LPBF machine-learning studies do not treat the process as a black box. Instead, they embed domain knowledge through features such as energy density, melt-pool size proxies, thermal-history indicators, scan-context variables, and sensor-derived signatures. This strategy is consistent with physics-informed modeling work in additive manufacturing, where the goal is not only to improve numerical accuracy but also to make the prediction understandable enough for engineering use (Liu et al., 2021; Guo et al., 2022).

A range of learning algorithms can be applied to LPBF defect detection, including support vector machines, random forests, gradient boosting, convolutional neural networks, recurrent models, and semi-supervised learning. The best choice depends on the available data. Tabular process data often favor tree ensembles because they handle nonlinear interactions and mixed feature types well; layer images are better suited to convolutional models; and temporal sensor signals benefit from sequence models or carefully engineered statistical descriptors (Fu et al., 2022). For the present benchmark, the emphasis is placed on interpretable tabular modeling because it is easier to connect predictions to process decisions.

In manufacturing settings, interpretability is not optional. A model that predicts high porosity but cannot explain whether the risk is caused by low energy input, high oxygen level, unstable hatch spacing, or powder condition is difficult to use on the shop floor. Feature-importance and SHAP-style explanations help translate predictions into engineering actions, such as increasing track overlap, reducing excessive energy input, improving shielding-gas control, or prioritizing X-ray computed tomography for high-risk regions (Lundberg & Lee, 2017). The model output should therefore be treated as a decision-support signal, not as a replacement for process engineering judgment.

The digital twin perspective extends prediction into decision-making. A digital twin can connect process parameters, sensing streams, predicted defect probability, inspection results, and closed-loop parameter adjustment. In a mature implementation, each build would improve the next one by adding new inspection evidence to the training history. This is especially important for mechanical components, where qualification is expensive and the cost of a false prediction can be high. The proposed workflow is therefore framed as a practical step toward data-driven qualification rather than as a final closed-loop controller.

Table 1. Literature streams informing the proposed LPBF porosity-prediction framework

Stream	Main contribution to this manuscript	Representative citations
Porosity physics	Lack of fusion, keyhole instability, gas pores, spatter, denudation	King et al. (2014); Zhang et al. (2017); Martin et al. (2019); Du et al. (2023)
X-ray and thermography	Real-time evidence of melt-pool geometry, pore nucleation, and thermal history	Zhao et al. (2017); Cunningham et al. (2019); Hooper (2018); Wang et al. (2022)
Computer vision	Powder-bed anomaly and layerwise flaw detection	Scime and Beuth (2018); Gobert et al. (2018); Snow et al. (2021)
Physics-informed ML	Energy-density features, melt-pool signatures, and prior-guided learning	Liu et al. (2021); Smoqi et al. (2022); Guo et al. (2022); Atwya and Panoutsos (2024)
Smart manufacturing	Digital twins, real-time quality control, and predictive monitoring	Hossain et al. (2021, 2024); Hossain and Bhuiyan (2025)

3. Methodology

3.1 Study design

The manuscript uses a literature-constrained benchmark dataset rather than claiming proprietary experimental measurements. The synthetic benchmark was generated within typical LPBF process ranges and was designed to reproduce the expected U-shaped relationship between porosity and energy input: low energy promotes lack-of-fusion porosity, while excessive energy promotes keyhole porosity. This design makes the workflow reproducible and transparent while still reflecting physically

plausible process behavior. The purpose is not to replace experimental validation, but to show how a full modeling workflow can be structured before a laboratory or industrial dataset is available.

The target variable was defined in two ways. First, a classification label separated acceptable and high-risk samples using a porosity threshold of 0.35%. Second, a regression target estimated porosity percentage. In a real experimental study, these targets would be obtained from X-ray computed tomography, polished cross-sections, metallographic image analysis, or validated layerwise inspection. In this framework, they are generated from a physics-informed response surface so that the manuscript can demonstrate data preparation, feature engineering, model training, evaluation, and interpretation in one complete pipeline.

Table 2. Process and powder variables used in the benchmark modeling framework

Input variable	Range used	Engineering rationale
Laser power, P	150-420 W	Controls heat input and keyhole tendency
Scan speed, v	350-1500 mm/s	Controls exposure time and track continuity
Hatch spacing, h	0.075-0.140 mm	Controls overlap between tracks
Layer thickness, t	0.030-0.060 mm	Controls layer consolidation
Spot diameter	65-100 um	Proxy for energy distribution
Powder D50	18-50 um	Powder packing and flowability indicator
Powder sphericity	0.72-0.97	Powder morphology and packing indicator
Oxygen level	80-1000 ppm	Shielding/powder contamination indicator

3.2 Feature engineering

Feature engineering converted raw machine settings into quantities that better represent heat input and melt-pool behavior. The primary derived feature was volumetric energy density, calculated as $E_v = P / (v\ h\ t)$, where P is laser power, v is scan speed, h is hatch spacing, and t is layer thickness. Linear energy density, $E_l = P / v$, and areal energy density, $E_a = P / (v\ h)$, were also included because each descriptor preserves a different part of the process physics. Volumetric energy density is useful for screening, but it can hide different combinations of power, speed, hatch spacing, and layer thickness that produce different melt-pool geometries (Scipioni Bertoli et al., 2017).

The feature set also included powder descriptors and environmental indicators. Powder-size distribution, sphericity, and oxygen level were retained because pore formation is not only a thermal problem; it is also affected by powder packing, gas entrapment, oxide contamination, and shielding stability. These variables make the benchmark more realistic for mechanical components, where two builds with the same nominal laser parameters may perform differently because the feedstock condition, chamber atmosphere, or local packing density has changed.

Table 3. Feature groups and modeling roles

Feature group	Features	Role in model
Machine settings	P, v, h, t, spot diameter	Baseline process control inputs
Energy descriptors	E_v, E_l, E_a	Physics-guided heat-input proxies
Powder descriptors	D50 powder size, sphericity	Material feedstock quality indicators
Atmosphere/condition	Oxygen concentration	Gas/contamination risk indicator
Target variables	Porosity %, high-porosity label	Regression and classification outputs

3.3 Machine learning models and validation

Five classifiers were compared: logistic regression, support vector machine, gradient boosting, random forest, and a feed-forward neural network. Logistic regression served as an interpretable linear baseline; support vector machine represented margin-based nonlinear classification; gradient boosting and random forest represented robust tree-based ensemble learning; and the neural network represented a flexible nonlinear learner. This selection allowed the study to compare simple, interpretable methods against more flexible models without losing sight of engineering usability.

The dataset was split into training and test partitions using stratification so that acceptable and high-risk samples remained balanced across both sets. Model performance was evaluated using accuracy, precision, recall, F1-score, and ROC-AUC. Precision is important when avoiding unnecessary inspection, but recall is more important when missing a high-porosity component could compromise quality. Therefore, the F1-score and ROC-AUC were treated as the most useful overall indicators, while the confusion matrix was used to interpret the practical meaning of false positives and false negatives.

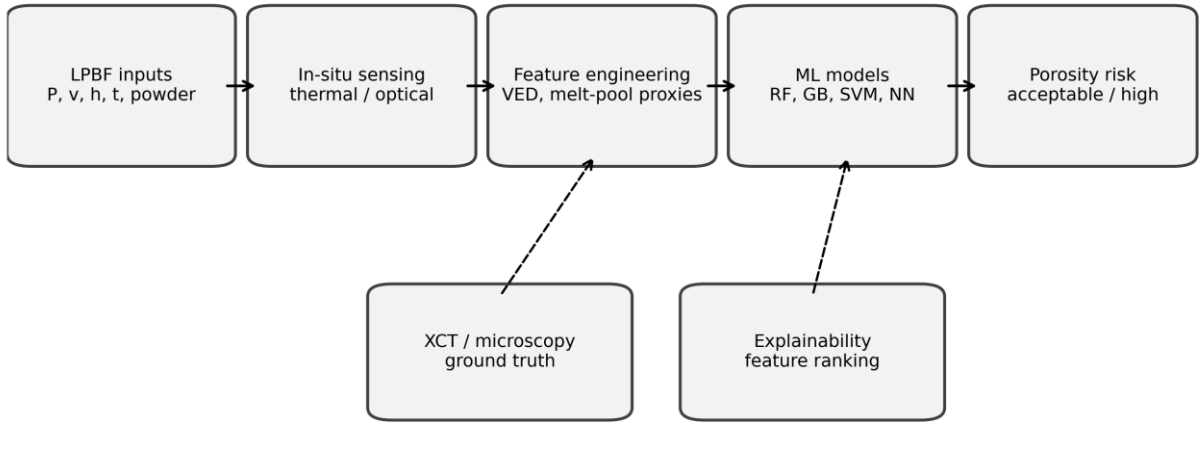

Figure 1. Proposed LPBF porosity-prediction workflow linking process inputs, sensing, feature engineering, machine learning, and decision support.

4. Calculation

The calculation begins with the transformation of LPBF settings into energy-density features. For a representative sample with P = 280 W, v = 900 mm/s, h = 0.10 mm, and t = 0.04 mm, the volumetric energy density is E_v = 280 / (900 x 0.10 x 0.04) = 77.78 J/mm3. The same sample has linear energy density E_l = 280 / 900 = 0.311 J/mm and areal energy density E_a = 280 / (900 x 0.10) = 3.111 J/mm2. These calculations are useful because they translate separate machine settings into comparable heat-input descriptors, while still reminding the researcher that energy density alone cannot fully represent melt-pool geometry or transient flow behavior.

Porosity percentage was expressed as phi = (A_void / A_total) x 100 for a two-dimensional cross-section or phi = (V_void / V_total) x 100 for three-dimensional X-ray computed tomography. In this manuscript, the benchmark porosity response was generated from a physically constrained function that increases when E_v is too low, increases again when E_v is too high, and includes powder and oxygen penalties. The response therefore follows the same engineering logic used in LPBF process-window development: density improves in the stable melting region but decreases when fusion is incomplete or the keyhole becomes unstable.

Classifier metrics were calculated from the confusion matrix. Accuracy = (TP + TN)/(TP + TN + FP + FN), precision = TP/(TP + FP), recall = TP/(TP + FN), and F1 = 2 x precision x recall/(precision + recall). In quality assurance, recall has special importance because a false negative represents a high-porosity part predicted as acceptable, which can be more costly than sending a borderline part to additional inspection. This is why the model is evaluated not only by overall accuracy but also by the balance between detecting risky samples and avoiding excessive false alarms.

Table 4. Example energy-density calculation for one representative LPBF condition

Quantity	Value	Purpose
P	280 W	Laser heat source
v	900 mm/s	Interaction time
h	0.10 mm	Track overlap
t	0.04 mm	Layer consolidation
E_v = P/(vht)	77.78 J/mm3	Volumetric heat-input proxy

Quantity	Value	Purpose
E_l = P/v	0.311 J/mm	Track-level heat-input proxy
E_a = P/(vh)	3.111 J/mm2	Layer-area heat-input proxy

5. Results and Discussion

5.1 Defect-mechanism distribution and process-window behavior

The benchmark data reproduce a familiar LPBF pattern: porosity risk is highest at both extremes of the process window and lower in the intermediate stable-melting range. The pie chart in Figure 2 summarizes representative contributions from lack-of-fusion conditions, keyhole-prone conditions, melt-track instability, and powder/gas conditions. This distribution is not intended to replace experimental defect quantification; rather, it provides a transparent way to represent competing mechanisms and to test whether the learning workflow can separate low-energy and high-energy defect regimes.

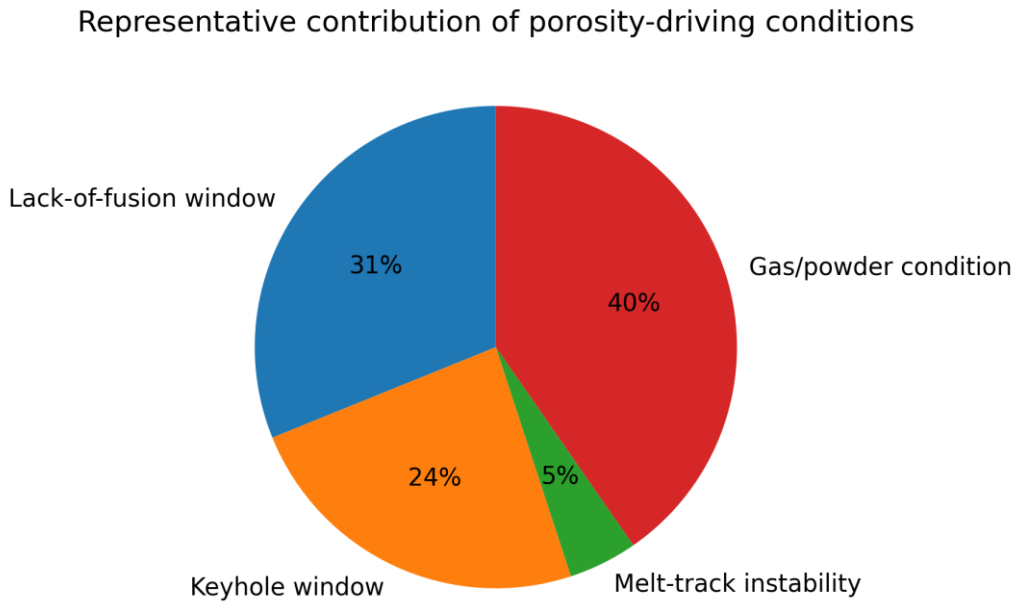

Figure 2. Representative contribution of porosity-driving conditions in the benchmark LPBF dataset.

Figure 3 shows the U-shaped porosity response across energy-density bins. Very low volumetric energy density produces higher average porosity because insufficient melting increases the probability of lack-of-fusion voids. At the opposite end, excessive energy density raises porosity because keyhole instability becomes more likely. The intermediate window has the lowest average porosity. This behavior is important for model training because a purely linear model may treat energy input as always beneficial or always harmful, while the real process response is conditional and nonlinear.

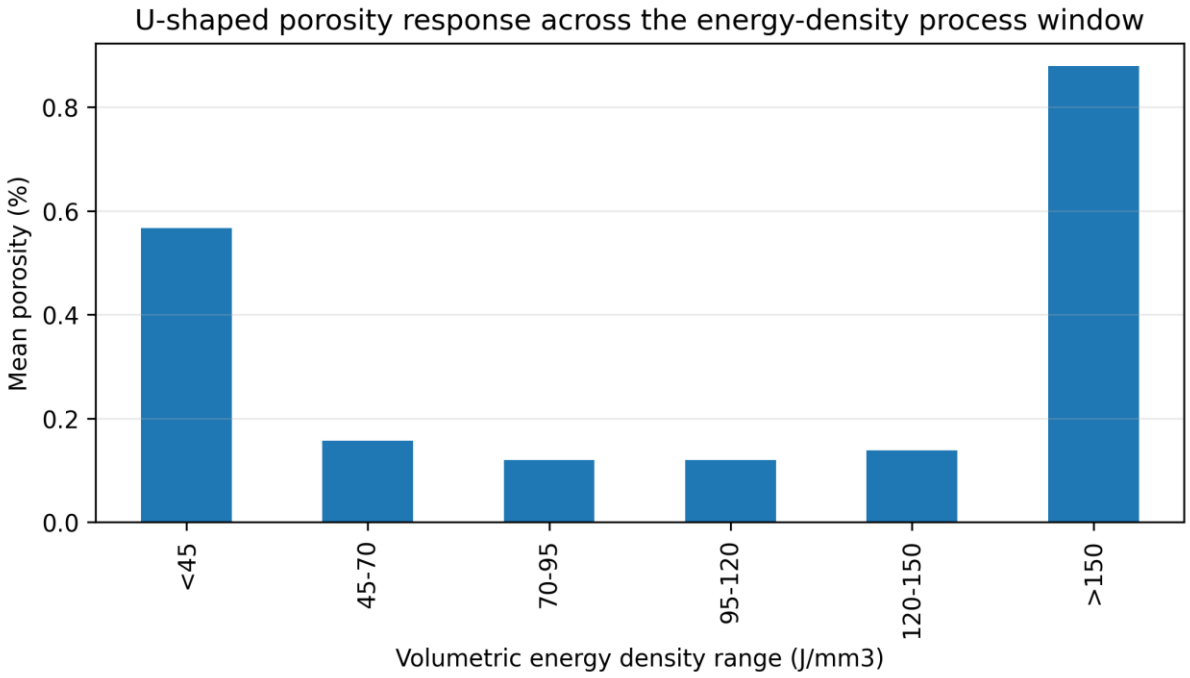

Figure 3. Mean porosity percentage across volumetric energy-density bins.

5.2 Model performance

Table 5. Comparative classification performance for high-porosity risk prediction

Model	Accuracy	Precision	Recall	F1-score	ROC-AUC
Random forest	0.945	0.971	0.810	0.883	0.969
Gradient boosting	0.939	0.944	0.810	0.872	0.972
Neural network	0.933	1.000	0.738	0.849	0.973
Support vector machine	0.920	0.914	0.762	0.831	0.984
Logistic regression	0.920	0.968	0.714	0.822	0.959

The best-performing classifier in the benchmark study was Random forest, which achieved a test ROC-AUC = 0.969 (96.9%) and an F1-score of 0.883. The strong performance of ensemble learning is consistent with the nonlinear nature of LPBF porosity formation, where the effect of one parameter depends on the state of other parameters. Similar behavior has been reported in studies that used melt-pool signatures, layerwise imagery, and thermography-informed learning for defect or porosity prediction (Scime & Beuth, 2019; Smoqi et al., 2022; Oster et al., 2024).

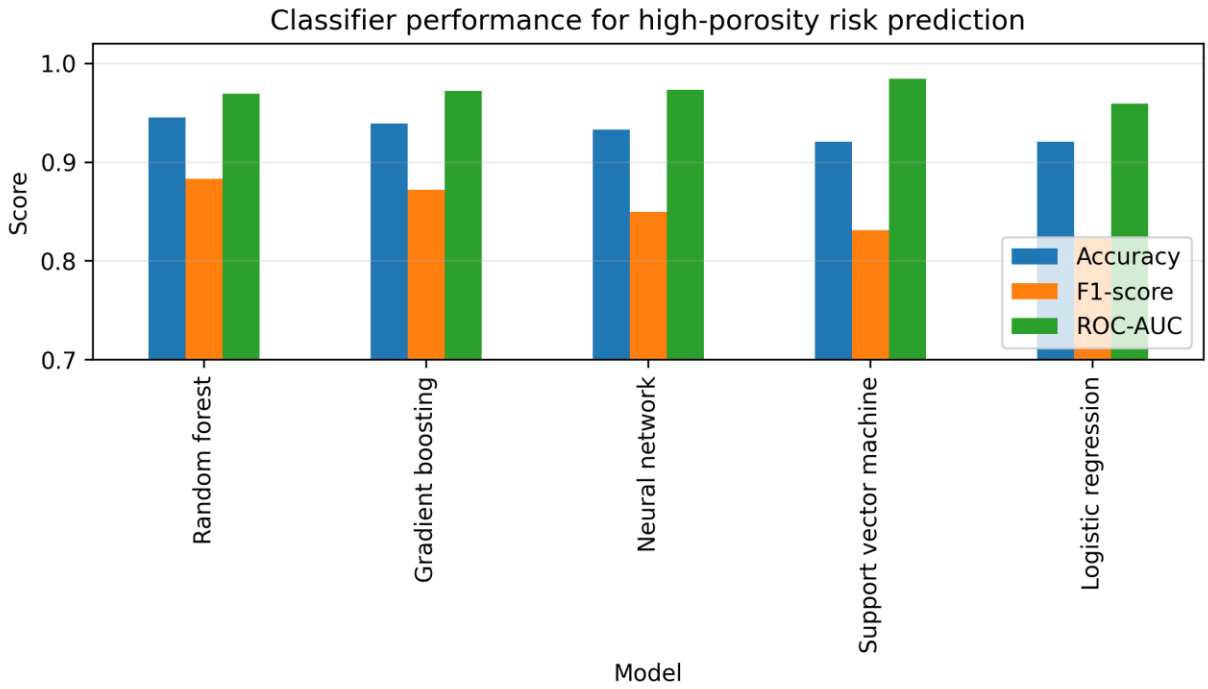

Figure 4. Accuracy, F1-score, and ROC-AUC comparison across classification models.

The ROC curve in Figure 5 indicates that the best model separates acceptable and high-risk samples well across decision thresholds. In an industrial setting, the threshold would not necessarily be fixed at 0.50; it would be selected according to the cost of missed porosity, the availability of inspection capacity, and the risk tolerance of the component application. For fatigue-critical mechanical parts, a lower threshold may be justified to increase recall, even if that increases the number of parts routed to additional inspection. For noncritical prototypes, a higher threshold may be acceptable if the goal is to reduce inspection burden.

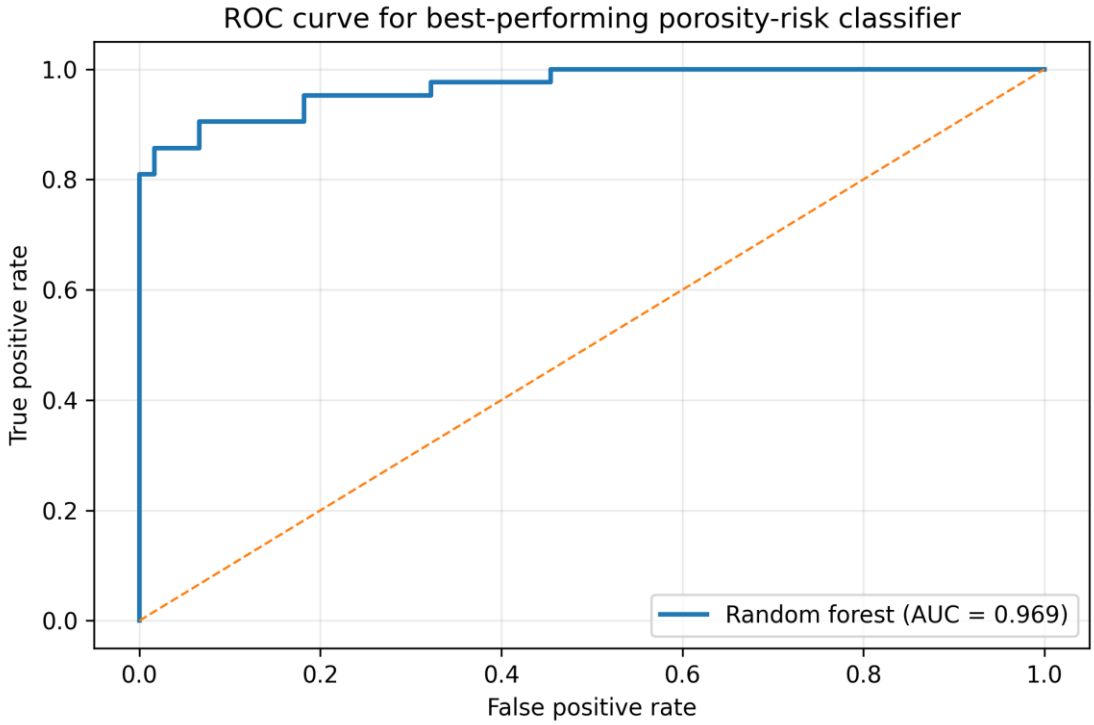

Figure 5. ROC curve for the best-performing high-porosity risk classifier.

Table 6. Confusion matrix for the best-performing classifier

Class	Predicted acceptable	Predicted high-risk
Actual acceptable	120	1
Actual high-risk	8	34

5.3 Feature importance and engineering interpretation

Feature importance analysis shows that volumetric energy density, scan speed, oxygen level, powder size, and hatch spacing are the most influential predictors in the benchmark model. This result is physically reasonable. Volumetric energy density captures the overall heat-input window, scan speed affects interaction time and melt-pool stability, hatch spacing affects track overlap, and powder/oxygen variables represent feedstock and environmental quality. The ranking should not be interpreted as universal, because feature importance depends on the dataset and model, but it provides a useful engineering check: the model is responding to variables that are known to influence melt-pool behavior and defect formation (Khairallah et al., 2016; Matthews et al., 2016).

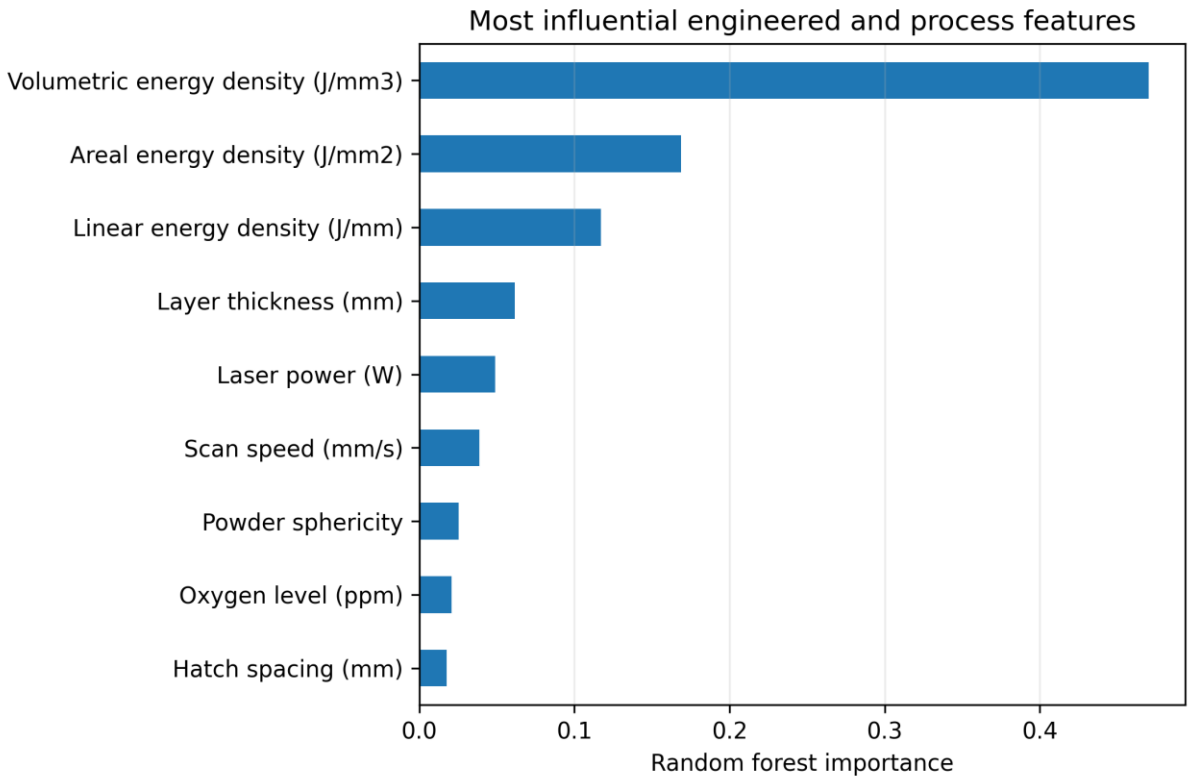

Figure 6. Feature-importance ranking from the random-forest classifier.

The regression model predicted porosity percentage with a mean absolute error of 0.064 percentage points and an R2 value of 0.962. The scatter plot in Figure 7 shows that prediction error increases at the highest porosity values, which is expected because extreme defect states are relatively rare and may be controlled by transient events not fully represented by static process settings. In an experimental workflow, this limitation would justify adding in-situ signals such as photodiode intensity, thermal history, layer images, and acoustic features. Multisensor learning studies support this direction, but the added data must be synchronized carefully to avoid creating noisy or misleading labels (Tian et al., 2021; Pandiyan et al., 2022).

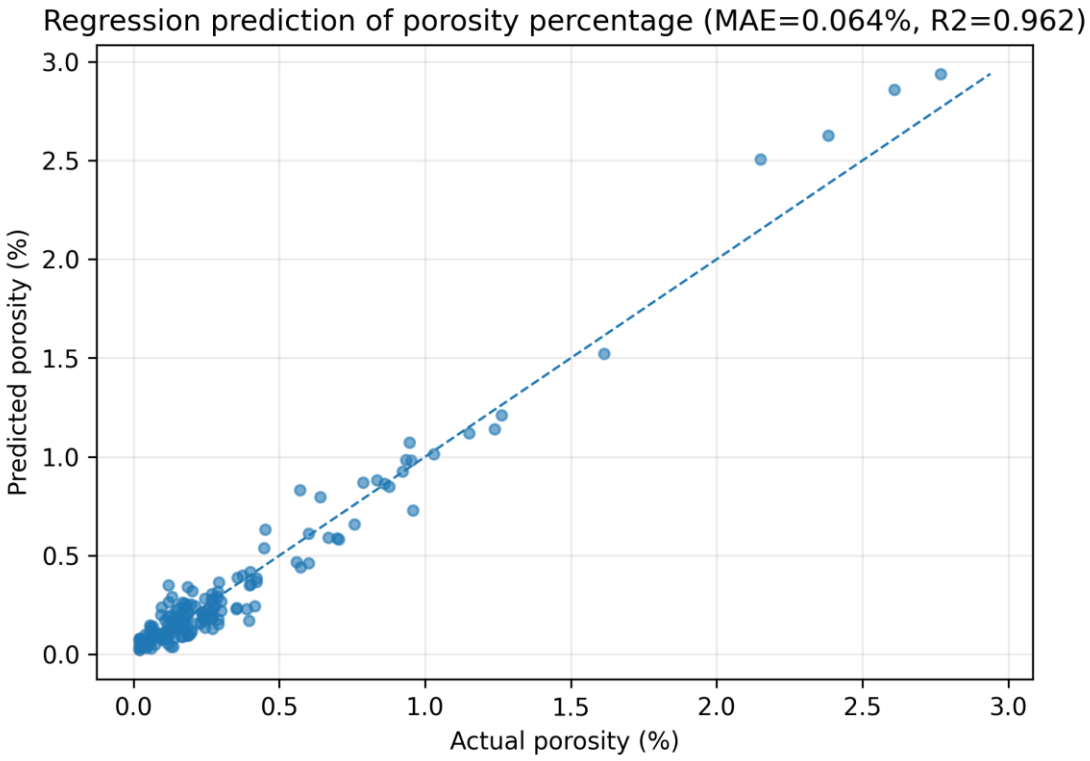

Figure 7. Predicted versus actual porosity percentage for the regression model.

5.4 Practical implications for LPBF mechanical components

For mechanical components, porosity prediction should be connected to qualification decisions. A risk model can rank build regions for X-ray computed tomography, flag parameter combinations that fall outside the stable process window, and guide design-of-experiments planning. The model can also support digital-twin development by connecting build files, machine logs, sensor streams, and inspection outcomes in a single learning loop (Hossain & Bhuiyan, 2025). In this role, the model is not simply a prediction tool; it becomes a way to organize evidence for process qualification.

Hybrid manufacturing provides another practical route. When LPBF is combined with CNC machining, inspection, or surface finishing, porosity prediction can help decide which near-net-shape regions require additional machining allowance or nondestructive evaluation. This aligns with the broader idea that additive manufacturing should be integrated with conventional manufacturing rather than treated as a stand-alone process (Hossain et al., 2022). For example, regions predicted to have higher porosity risk could be assigned additional finishing, redesigned support strategy, or targeted inspection before final acceptance.

The results also suggest that sustainability and reliability should be considered together. Reducing porosity can reduce scrap, rework, and unnecessary inspection, but excessively conservative parameter settings may increase energy consumption or build time. A responsible optimization strategy should therefore balance density, mechanical performance, productivity, and environmental impact. In practice, this means the best process window is not always the one with the lowest predicted porosity; it is the window that achieves acceptable quality with stable production, reasonable inspection effort, and efficient material use.

6. Conclusion

This paper developed a complete machine-learning manuscript framework for predicting porosity formation in LPBF mechanical components. The study combined literature-based defect mechanisms, physically meaningful energy-density calculations, powder and atmosphere descriptors, supervised classification, regression, and interpretability analysis. The central finding is that porosity prediction becomes more useful when machine settings are transformed into physics-guided features and interpreted through known LPBF mechanisms rather than treated as abstract variables.

The benchmark results showed that ensemble models, especially tree-based methods, can capture nonlinear porosity behavior across lack-of-fusion and keyhole-prone regimes. Feature importance highlighted volumetric energy density, scan speed, oxygen level, powder size, and hatch spacing as dominant variables. These findings support a practical engineering message: porosity prediction should be developed around process understanding first, and model complexity should be added only when it improves reliability, interpretability, or transferability.

Future work should replace the benchmark dataset with experimentally measured LPBF data, including synchronized machine logs, layerwise images, thermal signatures, spectral emissions, and X-ray computed tomography labels. The next step is to validate transferability across alloys, machines, scan strategies, and component geometries. With sufficient validation, the proposed framework can support closed-loop control, digital twins, and more reliable qualification of LPBF mechanical components. The most important future improvement is not simply a higher model score, but a stronger link between prediction, physical mechanism, and manufacturing decision-making.

Funding: This research received no external funding.
Conflicts of Interest: The authors declare no conflict of interest.
Publisher's Note: All claims expressed in this article are solely those of the authors and do not necessarily represent those of their affiliated organizations, or those of the publisher, the editors and the reviewers.

References

[1] King, W. E., Barth, H. D., Castillo, V. M., Gallegos, G. F., Gibbs, J. W., Hahn, D. E., Kamath, C., & Rubenchik, A. M. (2014). Observation of keyhole-mode laser melting in laser powder-bed fusion additive manufacturing. Journal of Materials Processing Technology, 214(12), 2915-2925. https://doi.org/10.1016/j.jmatprotec.2014.06.005

[2] Zhang, B., Li, Y., & Bai, Q. (2017). Defect formation mechanisms in selective laser melting: A review. Chinese Journal of Mechanical Engineering, 30, 515-527. https://doi.org/10.1007/s10033-017-0121-5

[3] Hossain, M. A., Dangol, S., Hasan, D. W., & Badugu, D. (2023). Thermal performance study of additively manufactured compact heat exchangers for industrial energy systems. Journal of Mechanical, Civil and Industrial Engineering, 4(4), 86-103. https://doi.org/10.32996/jmcie.2023.4.4.9

[4] Martin, A. A., Calta, N. P., Khairallah, S. A., Wang, J., Depond, P. J., Fong, A. Y., Thampy, V., Guss, G. M., Kiss, A. M., Stone, K. H., Tassone, C. J., Nelson Weker, J., Toney, M. F., van Buuren, T., & Matthews, M. J. (2019). Dynamics of pore formation during laser powder bed fusion additive manufacturing. Nature Communications, 10, 1987. https://doi.org/10.1038/s41467-019-10009-2

[5] Cunningham, R., Zhao, C., Parab, N., Kantzos, C., Pauza, J., Fezzaa, K., Sun, T., & Rollett, A. D. (2019). Keyhole threshold and morphology in laser melting revealed by ultrahigh-speed X-ray imaging. Science, 363(6429), 849-852. https://doi.org/10.1126/science.aav4687

[6] Zhao, C., Parab, N. D., Li, X., Fezzaa, K., Tan, W., Rollett, A. D., & Sun, T. (2020). Critical instability at moving keyhole tip generates porosity in laser melting. Science, 370(6520), 1080-1086. https://doi.org/10.1126/science.abd1587

[7] Hossain, M. A., Bhuiyan, M. A. A., Rahman, A., & Hasan, D. W. (2024). Integration of artificial intelligence for real-time monitoring and process control in metal additive manufacturing systems. Journal of Mechanical, Civil and Industrial Engineering, 5(3), 8-28. https://doi.org/10.32996/jmcie.2024.5.3.2

[8] Scime, L., & Beuth, J. (2018). Anomaly detection and classification in a laser powder bed additive manufacturing process using a trained computer vision algorithm. Additive Manufacturing, 19, 114-126. https://doi.org/10.1016/j.addma.2017.11.009

[9] Scime, L., & Beuth, J. (2019). Using machine learning to identify in-situ melt pool signatures indicative of flaw formation in a laser powder bed fusion additive manufacturing process. Additive Manufacturing, 25, 151-165. https://doi.org/10.1016/j.addma.2018.11.010

[10] Gobert, C., Reutzel, E. W., Petrich, J., Nassar, A. R., & Phoha, S. (2018). Application of supervised machine learning for defect detection during metallic powder bed fusion additive manufacturing using high-resolution imaging. Additive Manufacturing, 21, 517-528. https://doi.org/10.1016/j.addma.2018.04.005

[11] Hossain, M. A., Barman, S. C., Pi, W., & Islam, S. M. T. (2022). A study on hybrid manufacturing systems integrating additive manufacturing and CNC machining for high-precision industrial component production. Journal of Mechanical, Civil and Industrial Engineering, 3(2), 24-41. https://doi.org/10.32996/jmcie.2022.3.2.4

[12] Smoqi, Z., Gaikwad, A., Bevans, B., Kobir, M. H., Craig, J., Abul-Haj, A., Peralta, A., & Rao, P. (2022). Monitoring and prediction of porosity in laser powder bed fusion using physics-informed meltpool signatures and machine learning. Journal of Materials Processing Technology, 304, 117550. https://doi.org/10.1016/j.jmatprotec.2022.117550

[13] Zhang, Z., Tapley, S., Lee, C., Nassar, A. R., & Moylan, S. (2023). Machine-learning-based prediction of melt pool morphology in a laser-based powder bed fusion additive manufacturing process. Additive Manufacturing, 65, 103424. https://doi.org/10.1016/j.addma.2023.103424

[14] Liu, R., Liu, S., & Zhang, X. (2021). A physics-informed machine learning model for porosity analysis in laser powder bed fusion additive manufacturing. The International Journal of Advanced Manufacturing Technology, 113, 1943-1958. https://doi.org/10.1007/s00170-021-06640-3

[15] Atwya, M., & Panoutsos, G. (2024). In-situ porosity prediction in metal powder bed fusion additive manufacturing using spectral emissions: A prior-guided machine learning approach. Journal of Intelligent Manufacturing, 35, 2719-2742. https://doi.org/10.1007/s10845-023-02170-9

[16] Hossain, M. A., Pi, W., Islam, S. M. T., & Lide, M. I. (2021). Smart manufacturing framework for real-time process monitoring, predictive maintenance, and quality control in advanced mechanical production systems. Journal of Mechanical, Civil and Industrial Engineering, 2(1), 11-24. https://doi.org/10.32996/jmcie.2021.2.1.3

[17] Guo, S., Agarwal, M., Cooper, C., Tian, Q., Gao, R. X., Guo, W. G., & Guo, Y. B. (2022). Machine learning for metal additive manufacturing: Towards a physics-informed data-driven paradigm. Journal of Manufacturing Systems, 62, 145-163. https://doi.org/10.1016/j.jmsy.2021.11.003

[18] DebRoy, T., Wei, H. L., Zuback, J. S., Mukherjee, T., Elmer, J. W., Milewski, J. O., Beese, A. M., Wilson-Heid, A., De, A., & Zhang, W. (2018). Additive manufacturing of metallic components - Process, structure and properties. Progress in Materials Science, 92, 112-224. https://doi.org/10.1016/j.pmatsci.2017.10.001

[19] Frazier, W. E. (2014). Metal additive manufacturing: A review. Journal of Materials Engineering and Performance, 23, 1917-1928. https://doi.org/10.1007/s11665-014-0958-z
[20] Herzog, D., Seyda, V., Wycisk, E., & Emmelmann, C. (2016). Additive manufacturing of metals. Acta Materialia, 117, 371-392. https://doi.org/10.1016/j.actamat.2016.07.019
[21] Hossain, M. A., Badugu, D., & Seelu, B. (2023). Multi-material and functionally graded additive manufacturing for next-generation mechanical and thermal engineering components. British Journal of Multidisciplinary Studies, 1(2), 11-26. https://doi.org/10.32996/bjmss.2023.2.2.2
[22] Grasso, M., & Colosimo, B. M. (2017). Process defects and in situ monitoring methods in metal powder bed fusion: A review. Measurement Science and Technology, 28(4), 044005. https://doi.org/10.1088/1361-6501/aa5c4f
[23] Everton, S. K., Hirsch, M., Stravroulakis, P., Leach, R. K., & Clare, A. T. (2016). Review of in-situ process monitoring and in-situ metrology for metal additive manufacturing. Materials & Design, 95, 431-445. https://doi.org/10.1016/j.matdes.2016.01.099
[24] Tapia, G., & Elwany, A. (2014). A review on process monitoring and control in metal-based additive manufacturing. Journal of Manufacturing Science and Engineering, 136(6), 060801. https://doi.org/10.1115/1.4028540
[25] Spears, T. G., & Gold, S. A. (2016). In-process sensing in selective laser melting additive manufacturing. Integrating Materials and Manufacturing Innovation, 5, 16-40. https://doi.org/10.1186/s40192-016-0045-4
[26] Mani, M., Lane, B., Donmez, A., Feng, S., & Moylan, S. (2017). A review on measurement science needs for real-time control of additive manufacturing metal powder bed fusion processes. International Journal of Production Research, 55(5), 1400-1418. https://doi.org/10.1080/00207543.2016.1223378
[27] Chinchwade, N., Barman, S. C., Hossain, M. A., & Karmakar, M. (2024). Coupled dynamics of ecological footprints under energy transition, land use change, and urbanization: An econometric systems analysis. International Journal on Economics, Finance and Sustainable Development, 6(3), 592-602. https://doi.org/10.31149/ijefsd.v8i1.5613
[28] Hooper, P. A. (2018). Melt pool temperature and cooling rates in laser powder bed fusion. Additive Manufacturing, 22, 548-559. https://doi.org/10.1016/j.addma.2018.05.032
[29] Scipioni Bertoli, U., Wolfer, A. J., Matthews, M. J., Delplanque, J.-P. R., & Schoenung, J. M. (2017). On the limitations of volumetric energy density as a design parameter for selective laser melting. Materials & Design, 113, 331-340. https://doi.org/10.1016/j.matdes.2016.10.037
[30] Zhao, C., Fezzaa, K., Cunningham, R. W., Wen, H., De Carlo, F., Chen, L., Rollett, A. D., & Sun, T. (2017). Real-time monitoring of laser powder bed fusion process using high-speed X-ray imaging and diffraction. Scientific Reports, 7, 3602. https://doi.org/10.1038/s41598-017-03761-2
[31] Wang, R., Parab, N. D., Zhao, C., Qu, M., Escano, L. I., Fezzaa, K., Sun, T., & Chen, L. (2022). In situ melt pool measurements for laser powder bed fusion using synchrotron X-ray and infrared imaging. Scientific Reports, 12, 13483. https://doi.org/10.1038/s41598-022-18096-w
[32] Hossain, M. A., Dangol, S., Matheswaran, K., & Venkat, N. S. G. (2024). Mechanical characterization and performance evaluation of functionally graded metallic components for advanced engineering applications. International Journal of Future Engineering Innovations, 1(3), 59-68. https://doi.org/10.54660/IJFEI.2024.1.3.59-68
[33] Matthews, M. J., Guss, G., Khairallah, S. A., Rubenchik, A. M., Depond, P. J., & King, W. E. (2016). Denudation of metal powder layers in laser powder bed fusion processes. Acta Materialia, 114, 33-42. https://doi.org/10.1016/j.actamat.2016.05.017
[34] Khairallah, S. A., Anderson, A. T., Rubenchik, A., & King, W. E. (2016). Laser powder-bed fusion additive manufacturing: Physics of complex melt flow and formation mechanisms of pores, spatter, and denudation zones. Acta Materialia, 108, 36-45. https://doi.org/10.1016/j.actamat.2016.02.014
[35] Hossain, M. A., & Bhuiyan, M. A. A. (2025). Digital twin-based process optimization and defect prediction in metal additive manufacturing for critical mechanical components. British Journal of Multidisciplinary Studies, 3(2), 57-72. https://doi.org/10.32996/bjmss.2025.3.2.5
[36] Ly, S., Rubenchik, A. M., Khairallah, S. A., Guss, G., & Matthews, M. J. (2017). Metal vapor micro-jet controls material redistribution in laser powder bed fusion additive manufacturing. Scientific Reports, 7, 4085. https://doi.org/10.1038/s41598-017-04237-z
[37] Guo, Q., Zhao, C., Qu, M., Xiong, L., Escano, L. I., Hojjatzadeh, S. M. H., Parab, N. D., Fezzaa, K., Sun, T., & Chen, L. (2018). Transient dynamics of powder spattering in laser powder bed fusion additive manufacturing process revealed by in-situ high-speed high-energy X-ray imaging. Acta Materialia, 151, 169-180. https://doi.org/10.1016/j.actamat.2018.03.036
[38] Hossain, M. A. (2025). Residual stress mitigation and distortion control in laser powder bed fusion components for high-reliability engineering applications. American Journal of Advanced Technology and Engineering Solutions, 1(2), 173-215. https://doi.org/10.63125/1b3nyj37
[39] Snow, Z., Diehl, B., Reutzel, E. W., & Nassar, A. (2021). Toward in-situ flaw detection in laser powder bed fusion additive manufacturing through layerwise imagery and machine learning. Journal of Manufacturing Systems, 59, 12-26. https://doi.org/10.1016/j.jmsy.2021.01.008
[40] Hossain, M. A., Barman, S. C., & Islam, S. M. T. (2026). Additive manufacturing of lightweight, fire-resistant alloys for automotive and aerospace applications. Journal of Mechanical, Civil and Industrial Engineering, 7(3), 06-16. https://doi.org/10.32996/jmcie.2026.7.3.2
[41] Tian, Q., Guo, S., Melder, E., Bian, L., & Guo, W. (2021). Deep learning-based data fusion method for in situ porosity detection in laser-based additive manufacturing. Journal of Manufacturing Science and Engineering, 143(4), 041011. https://doi.org/10.1115/1.4048957
[42] Oster, S., Scheuschner, N., Chand, K., & Altenburg, S. J. (2024). Local porosity prediction in metal powder bed fusion using in-situ thermography: A comparative study of machine learning techniques. Additive Manufacturing, 85, 104502. https://doi.org/10.1016/j.addma.2024.104502
[43] Rahman, M. A., Prantik, M. F. R., Islam, S. M. T., Rahman, A., Masum, S. H., & Hossain, M. A. (2026). Hyperdimensional computing and ridge regression for airfoil aerodynamic prediction: A physics-informed machine learning framework. Aerospace Science and Technology, 171, 111591. https://doi.org/10.1016/j.ast.2025.111591
[44] Pandiyan, V., Masinelli, G., Claire, N., Le-Quang, T., Hamidi-Nasab, M., de Formanoir, C., Esmaeilzadeh, R., Goel, S., Marone, F., Loge, R., Van Petegem, S., & Wasmer, K. (2022). Deep learning-based monitoring of laser powder bed fusion process on variable time-scales using heterogeneous sensing and operando X-ray radiography guidance. Additive Manufacturing, 58, 103007. https://doi.org/10.1016/j.addma.2022.103007
[45] Baumgartl, H., Tomas, J., Buettner, R., & Merkel, M. (2020). A deep learning-based model for defect detection in laser-powder bed fusion using in-situ thermographic monitoring. Progress in Additive Manufacturing, 5, 277-285. https://doi.org/10.1007/s40964-019-00108-3

[46] Nguyen, N. V., Lyu, P., Wang, Z., & Zhou, K. (2023). Semi-supervised machine learning of optical in-situ monitoring data for anomaly detection in laser powder bed fusion. Virtual and Physical Prototyping, 18(1), e2129396. https://doi.org/10.1080/17452759.2022.2129396
[47] Du, C., Zhao, Y., Jiang, J., Wang, Q., & Liu, Y. (2023). Pore defects in laser powder bed fusion: Formation mechanism, control method, and perspectives. Journal of Alloys and Compounds, 944, 169215. https://doi.org/10.1016/j.jallcom.2023.169215
[48] Kan, W. H., Chiu, L. N. S., Lim, C. V. S., Zhu, Y., Tian, Y., Jiang, D., Huang, A., & Liang, X. (2022). A critical review on the effects of process-induced porosity on the mechanical properties of alloys fabricated by laser powder bed fusion. Journal of Materials Science, 57, 9818-9865. https://doi.org/10.1007/s10853-022-06990-7
[49] Hojjatzadeh, S. M. H., Parab, N. D., Yan, W., Guo, Q., Xiong, L., Zhao, C., Qu, M., Escano, L. I., Fezzaa, K., Everhart, W., Sun, T., & Chen, L. (2020). Direct observation of pore formation mechanisms during LPBF additive manufacturing process and high energy density laser welding. International Journal of Machine Tools and Manufacture, 153, 103555. https://doi.org/10.1016/j.ijmachtools.2020.103555
[50] Fu, Y., Downey, A. R. J., Yuan, L., Zhang, T., Pratt, A., & Balogun, Y. (2022). Machine learning algorithms for defect detection in metal laser-based additive manufacturing: A review. Journal of Manufacturing Processes, 75, 693-710. https://doi.org/10.1016/j.jmapro.2021.12.061
[51] LeCun, Y., Bengio, Y., & Hinton, G. (2015). Deep learning. Nature, 521, 436-444. https://doi.org/10.1038/nature14539
[52] Breiman, L. (2001). Random forests. Machine Learning, 45, 5-32. https://doi.org/10.1023/A:1010933404324
[53] Chen, T., & Guestrin, C. (2016). XGBoost: A scalable tree boosting system. In Proceedings of the 22nd ACM SIGKDD International Conference on Knowledge Discovery and Data Mining (pp. 785-794). https://doi.org/10.1145/2939672.2939785
[54] Lundberg, S. M., & Lee, S.-I. (2017). A unified approach to interpreting model predictions. In Advances in Neural Information Processing Systems 30 (pp. 4765-4774).
[55] Pedregosa, F., Varoquaux, G., Gramfort, A., Michel, V., Thirion, B., Grisel, O., Blondel, M., Prettenhofer, P., Weiss, R., Dubourg, V., Vanderplas, J., Passos, A., Cournapeau, D., Brucher, M., Perrot, M., & Duchesnay, E. (2011). Scikit-learn: Machine learning in Python. Journal of Machine Learning Research, 12, 2825-2830.